Prepared for submission to JHEP

Effects of Two Inert Scalar Doublets on Higgs Interactions and Electroweak Phase Transition

Amine Ahriche,[a] **Gaber Faisel,**[b,c] **Shu-Yu Ho,**[d] **Salah Nasri**[e] **and Jusak Tandean**[b]

[a] *Department of Physics, University of Jijel, PB 98 Ouled Aissa, DZ-18000 Jijel, Algeria.*

[b] *Department of Physics and Center for Theoretical Sciences, National Taiwan University, Taipei 106, Taiwan*

[c] *Egyptian Center for Theoretical Physics, Modern University for Information and Technology, Cairo, Egypt*

[d] *Department of Physics, California Institute of Technology, Pasadena, CA 91125, USA*

[e] *Physics Department, UAE University, POB 17551, Al Ain, United Arab Emirates.*

E-mail: aahriche@ictp.it, gfaisel@hep1.phys.ntu.edu.tw, sho3@caltech.edu, snasri@uaeu.ae.ac, jtandean@yahoo.com

Abstract: We study some implications of the presence of two inert scalar doublets which are charged under a dark Abelian gauge symmetry. Specifically, we investigate the effects of the new scalars on oblique electroweak parameters and on the interactions of the 125 GeV Higgs boson, especially its decay modes $h \to \gamma\gamma, \gamma Z$ and trilinear coupling, all of which will be probed with improved precision in future Higgs measurements. Moreover, we explore how the inert scalars may give rise to strongly first-order electroweak phase transition and also show its correlation with sizable modifications to the Higgs trilinear coupling.

Keywords: Inert doublets, Higgs decay, oblique parameters, electroweak phase transition.

Contents

1 Introduction

The recent discovery [1, 2] at the Large Hadron Collider (LHC) of a Higgs boson with mass around 125 GeV and other properties consistent with the expectations of the standard model (SM) serves as yet another confirmation that it is a remarkably successful theory. Nevertheless, it is widely believed that new physics beyond it is still necessary at least to account for the compelling experimental evidence for neutrino mass and the astronomical indications of dark matter [3].

Among a great many possibilities beyond the SM are those with enlarged scalar sectors. Scenarios incorporating a second Higgs doublet are of course highly popular in the literature [4, 5]. Of late models with three scalar doublets have also been gaining interest [6–9], as they can provide dark-matter candidates [8] and/or an important ingredient for the mechanism that generates neutrino mass [9].

In this paper we consider this three-doublet possibility, in particular that which involves two inert scalar doublets, besides the standard Higgs doublet, plus a dark

Abelian gauge symmetry. The extra scalar particles are inert in that they possess no direct couplings to a pair of exclusively SM fermions. However, being members of doublets, these scalars have interactions with SM gauge bosons at tree level. The new gauge group is dark in the sense that SM particles are not charged under it and that the associated gauge boson is taken to have vanishing kinetic-mixing with the hypercharge gauge boson.

We assume that the scalar sector is part of a more complete theory, such as has recently been explored in the context of a scotogenic scenario [9], where neutrinos acquire mass radiatively via their one-loop interactions with both new fermions and the inert scalars. Here we focus on these scalars, none of which is supposed to be a dark-matter candidate, and explore some implications of their presence. Specifically, we study constraints on the inert scalars from collider measurements on the Higgs boson and from electroweak precision data. In addition, we look at the potential impact of the scalars on the Higgs trilinear coupling, anticipating future experiments that will probe it sufficiently well. To evaluate the coupling, we will employ the Higgs effective potential derived at the one-loop level. Moreover, we examine how the new particles, which we choose to have sub-TeV masses, may give rise to strongly first-order electroweak phase transition (EWPT), which is needed for electroweak baryogenesis to explain the baryon asymmetry of the Universe. As it has been pointed out in the context of other models that the strength of EWPT could be correlated with sizable modifications to the Higgs trilinear coupling [10–12], our results will indicate how this may be realized in the presence of the new doublets.

The plan of the paper is as follows. In the next section, we describe the scalar Lagrangian and address some theoretical constraints on its parameters, especially from the requirements on vacuum stability. Since the extra scalar doublets couple to the standard Higgs and gauge bosons and include electrically-charged members, they contribute at the one-loop level to the Higgs decays $h \to \gamma\gamma$ and $h \to \gamma Z$ which have been under intense investigation at the LHC, the former channel having also been observed. We determine their rates in section 3, where we also start our numerical analysis by exploring the charged scalars' impact on these processes. In section 4, we calculate the contributions of the new doublets to the oblique electroweak observables S and T, on which experimental information is available. Sections 5 and 6 contain our treatment of the new scalars' effects on the trilinear Higgs couplings and on the electroweak phase transition, respectively. After deriving the relevant formulas, we perform further numerical work in these sections. In section 7, we discuss additional results and make our conclusions after combining different relevant constraints. A few appendices contain more discussions and formulas.

2 Scalar Sector

2.1 Lagrangian

Compared to the SM with the Higgs doublet Φ, the scalar sector is expanded with the addition of two doublets, η_1 and η_2. The theory also possesses a dark Abelian gauge symmetry, $\mathrm{U}(1)_D$, under which $\eta_{1,2}$ carry charges $+1$ and -1, respectively, whereas SM particles are not charged. Accordingly, one can express the renormalizable Lagrangian for the interactions of the scalars with each other and with the standard $\mathrm{SU}(2)_L \times \mathrm{U}(1)_Y$ gauge bosons, $W_{1,2,3}$ and B, as well as the $\mathrm{U}(1)_D$ gauge boson C, as

$$\mathcal{L} = (\mathcal{D}^\mu \Phi)^\dagger \mathcal{D}_\mu \Phi + (\mathcal{D}^\mu \eta_1)^\dagger \mathcal{D}_\mu \eta_1 + (\mathcal{D}^\mu \eta_2)^\dagger \mathcal{D}_\mu \eta_2 \; - \; \mathcal{V}, \tag{2.1}$$

where the covariant derivative $\mathcal{D}^\mu = \partial^\mu + (ig/2)\tau_j W_j^\mu + i g_Y \mathcal{Q}_Y B^\mu + i g_D \mathcal{Q}_C C^\mu$ also contains the gauge couplings g, g_Y, and g_D, Pauli matrices $\tau_{1,2,3}$, and $\mathrm{U}(1)_{Y,D}$ charge operators $\mathcal{Q}_{Y,C}$, while the scalar potential is

$$\begin{aligned}\mathcal{V} = {} & \mu_1^2 \Phi^\dagger \Phi + \mu_{21}^2 \eta_1^\dagger \eta_1 + \mu_{22}^2 \eta_2^\dagger \eta_2 + \tfrac{1}{2}\lambda_1 (\Phi^\dagger \Phi)^2 + \tfrac{1}{2}\lambda_{21} (\eta_1^\dagger \eta_1)^2 + \tfrac{1}{2}\lambda_{22} (\eta_2^\dagger \eta_2)^2 \\ & + \lambda_{31} \Phi^\dagger \Phi \eta_1^\dagger \eta_1 + \lambda_{32} \Phi^\dagger \Phi \eta_2^\dagger \eta_2 + \lambda_{41} \Phi^\dagger \eta_1 \eta_1^\dagger \Phi + \lambda_{42} \Phi^\dagger \eta_2 \eta_2^\dagger \Phi \\ & + \tfrac{1}{2}\left[\lambda_5 \Phi^\dagger \eta_1 \Phi^\dagger \eta_2 + \lambda_5^* \eta_1^\dagger \Phi \eta_2^\dagger \Phi\right] + \lambda_6 \eta_1^\dagger \eta_1 \eta_2^\dagger \eta_2 + \lambda_7 \eta_1^\dagger \eta_2 \eta_2^\dagger \eta_1 .\end{aligned} \tag{2.2}$$

Thus $\mathcal{Q}_C \Phi = 0$ and $\mathcal{Q}_C \eta_1(\eta_2) = +\eta_1(-\eta_2)$. The parameters $\mu_{1,2a}^2$ and $\lambda_{1,2a,3a,4a,6,7}$ with $a = 1, 2$ are necessarily real because of the hermiticity of $\mathcal{V}$, whereas λ_5 can be rendered real using the relative phase between Φ and $\eta_{1,2}$. Assuming that the $\mathrm{U}(1)_D$ symmetry stays intact, after electroweak symmetry breaking we can write

$$\Phi = \begin{pmatrix} 0 \\ \frac{1}{\sqrt{2}}(v + h) \end{pmatrix}, \qquad \eta_a = \begin{pmatrix} H_a^+ \\ \eta_a^0 \end{pmatrix}, \qquad \sqrt{2}\, \eta_a^0 = \mathrm{Re}\eta_a^0 + i\mathrm{Im}\eta_a^0 \,, \tag{2.3}$$

where h represents the physical Higgs boson, $v \simeq 246$ GeV is the vacuum expectation value (VEV) of Φ, and H_a^+ and η_a^0 denote, respectively, the electrically charged and neutral components of η_a, which has no VEV.

From the terms in $\mathcal{V}$ that are quadratic in the fields, it is straightforward to extract the mass eigenstates of the scalars. Thus the masses of h and $H_{1,2}^\pm$ at tree level are given by

$$\hat{m}_h^2 = \mu_1^2 + \tfrac{3}{2}\lambda_1 v^2, \quad m_{H_a}^2 = \mu_{2a}^2 + \tfrac{1}{2}\lambda_{3a} v^2. \tag{2.4}$$

The λ_5 part in eq. (2.2) causes mixing between the electrically neutral components η_1^0 and η_2^{0*}, which are then related to the mass eigenstates χ_1 and χ_2 according to

$$\begin{aligned}\begin{pmatrix} \eta_1^0 \\ \eta_2^{0*} \end{pmatrix} &= \begin{pmatrix} c_\theta & s_\theta \\ -s_\theta & c_\theta \end{pmatrix} \begin{pmatrix} \chi_1 \\ \chi_2 \end{pmatrix}, \qquad c_\theta = \cos\theta, \qquad s_\theta = \sin\theta, \\ \tan(2\theta) &= \frac{\lambda_5 v^2}{2m_{H_2}^2 - 2m_{H_1}^2 + (\lambda_{42} - \lambda_{41})\, v^2} \,,\end{aligned} \tag{2.5}$$

the resulting eigenmasses being given by

$$m^2_{\chi_{1,2}} = \tfrac{1}{2}\left(m^2_{H_1} + m^2_{H_2}\right) + \tfrac{1}{4}\left(\lambda_{41}+\lambda_{42}\right)v^2 \\ \mp \tfrac{1}{2}\sqrt{\left[m^2_{H_2} - m^2_{H_1} + \tfrac{1}{2}\left(\lambda_{42}-\lambda_{41}\right)v^2\right]^2 + \tfrac{1}{4}\lambda_5^2 v^4}\,. \tag{2.6}$$

Hence the $\mathrm{U}(1)_D$ charges of $\chi_{1,2}$ are the same as (opposite in sign to) that of η_1 (η_2) and $m_{\chi_1} \leq m_{\chi_2}$.

Alternatively, instead of χ_a, one can choose to deal with their real and imaginary parts,

$$\mathcal{S}_a = \sqrt{2}\,\mathrm{Re}\chi_a, \qquad \mathcal{P}_a = \sqrt{2}\,\mathrm{Im}\chi_a, \tag{2.7}$$

which are CP-even and CP-odd states, respectively, and share mass, $m_{\mathcal{S}_a} = m_{\mathcal{P}_a} = m_{\chi_a}$. From eq. (2.5), one then has in matrix form

$$\begin{pmatrix} \mathrm{Re}\eta_1^0 \\ \mathrm{Re}\eta_2^0 \\ \mathrm{Im}\eta_1^0 \\ \mathrm{Im}\eta_2^0 \end{pmatrix} = \begin{pmatrix} c_\theta & s_\theta & 0 & 0 \\ -s_\theta & c_\theta & 0 & 0 \\ 0 & 0 & c_\theta & s_\theta \\ 0 & 0 & s_\theta & -c_\theta \end{pmatrix} \begin{pmatrix} \mathcal{S}_1 \\ \mathcal{S}_2 \\ \mathcal{P}_1 \\ \mathcal{P}_2 \end{pmatrix}, \tag{2.8}$$

where the mixing matrix is orthogonal.

Later on, we will concentrate on the scenario in which λ_5 is negligible compared to the other λ's in $\mathcal{V}$, but does not vanish.[1] In that case, as eq. (2.5) indicates, the η_1^0-η_2^{0*} mixing is small, $\theta \ll 1$, provided that $\lambda_5 v^2 \ll 2m^2_{H_1} - 2m^2_{H_2} + \left(\lambda_{41}-\lambda_{42}\right)v^2$. Furthermore, one can see from eq. (2.6) that at the same time χ_1 and χ_2 can be close in mass if $\frac{1}{2}\lambda_5 v^2 \ll m^2_{H_1} - m^2_{H_2} + \frac{1}{2}\left(\lambda_{41}-\lambda_{42}\right)v^2 \ll m^2_{\chi_1}$.

2.2 Theoretical Constraints

The parameters of the scalar potential are subject to a number of theoretical constraints. The stability of the vacuum implies that $\mathcal{V}$ must be bounded from below. As shown in appendix A, with λ_5 being negligible, this entails that for $a = 1, 2$

$$\lambda_1 > 0, \quad \lambda_{2a} > 0, \quad \lambda_{3a} + \lambda^0_{4a} + \sqrt{\lambda_1\lambda_{2a}} > 0, \quad \lambda_6 + \lambda^0_7 + \sqrt{\lambda_{21}\lambda_{22}} > 0, \\ \sqrt{\lambda_1\lambda_{21}\lambda_{22}} + \sqrt{\lambda_1}\left(\lambda_6 + \lambda^0_7\right) + \sqrt{\lambda_{21}}\left(\lambda_{32} + \lambda^0_{42}\right) + \sqrt{\lambda_{22}}\left(\lambda_{31} + \lambda^0_{41}\right) \\ + \left[2\left(\sqrt{\lambda_1\lambda_{21}} + \lambda_{31} + \lambda^0_{41}\right)\left(\sqrt{\lambda_1\lambda_{22}} + \lambda_{32} + \lambda^0_{42}\right)\left(\sqrt{\lambda_{21}\lambda_{22}} + \lambda_6 + \lambda^0_7\right)\right]^{1/2} > 0, \tag{2.9}$$

where $\lambda^0_x \equiv \mathrm{Min}(0, \lambda_x)$.

The μ^2 and λ parameters in $\mathcal{V}$ also need to have such values that its minimum with the VEV of Φ (η_a) being nonzero (zero) is global. This is already guaranteed [7] by the positivity of the mass eigenvalues in eqs. (2.4) and (2.6).

[1] If the potential $\mathcal{V}$ is embedded in a scotogenic model, the nonvanishing of λ_5 is essential for generating the loop-induced neutrino masses [9].

In addition, the perturbativity of the theory implies that the magnitudes of the λ parameters need to be capped. Thus, in numerical work our choices for their ranges, to be specified later on, will meet the general requirement $|\lambda_x| < 8\pi$, in analogy to that in the two-Higgs-doublet case [13].

3 Restrictions from Collider Data

The kinetic portion of the Lagrangian in eq. (2.1) contains the interactions of the new scalars with the photon and weak bosons,

$$\begin{aligned}\mathcal{L} \supset\ & iH_a^+ \overleftrightarrow{\partial^\mu} H_a^- \left(eA_\mu - g_L Z_\mu\right) + H_a^+ H_a^- \left(eA - g_L Z\right)^2 \\ & + \frac{ig}{2c_\mathrm{w}} \left[c_{2\theta} \left(\chi_1^* \overleftrightarrow{\partial^\mu} \chi_1 - \chi_2^* \overleftrightarrow{\partial^\mu} \chi_2\right) + s_{2\theta} \left(\chi_1^* \overleftrightarrow{\partial^\mu} \chi_2 + \chi_2^* \overleftrightarrow{\partial^\mu} \chi_1\right)\right] Z_\mu + \frac{g^2}{4c_\mathrm{w}^2} \chi_a^* \chi_a Z^2 \\ & + \frac{ig}{\sqrt{2}} \left\{\left[c_\theta \left(H_1^+ \overleftrightarrow{\partial^\mu} \chi_1^* + H_2^+ \overleftrightarrow{\partial^\mu} \chi_2\right) + s_\theta \left(H_1^+ \overleftrightarrow{\partial^\mu} \chi_2^* - H_2^+ \overleftrightarrow{\partial^\mu} \chi_1\right)\right] W_\mu^- - \mathrm{H.c.}\right\} \\ & + \frac{g^2}{2} \left(H_a^+ H_a^- + \chi_a^* \chi_a\right) W^{+\mu} W_\mu^- \ , \end{aligned} \tag{3.1}$$

where summation over $a = 1, 2$ is implicit,

$$X \overleftrightarrow{\partial^\mu} Y = X \partial^\mu Y - Y \partial^\mu X \ , \qquad g_L = \frac{g}{2c_\mathrm{w}} \left(2s_\mathrm{w}^2 - 1\right) , \tag{3.2}$$

$c_\mathrm{w} = \cos\theta_\mathrm{w} = (1 - s_\mathrm{w}^2)^{1/2}$, with θ_w being the usual Weinberg angle, $c_{2\theta} = \cos(2\theta)$, and $s_{2\theta} = \sin(2\theta)$. One can alternatively write eq. (3.1) in terms of the real and imaginary components $\mathcal{S}_a$ and $\mathcal{P}_a$ of χ_a, which becomes more lengthy and are relegated to appendix B.

We now see that data from past colliders can lead to some constraints on the masses of the new scalars. Based on eq. (3.1), we may infer from the experimental widths of the W and Z bosons and the absence so far of evidence for nonstandard particles in their decay modes that for $a, b = 1, 2$

$$m_{H_a} + m_{\chi_b} > m_W, \qquad 2m_{H_a} > m_Z, \qquad m_{\chi_a} + m_{\chi_b} > m_Z. \tag{3.3}$$

The null results of direct searches for new particles at e^+e^- colliders also imply lower limits on these masses, especially those of the charged scalars. A recent investigation [14] concerning the effects of the corresponding particles in the simplest scotogenic model [15] on the relevant processes measured at LEP II suggests that such charged scalars may face significant constraints if their masses are below 100 GeV. For these reasons, in our numerical work we will generally consider the mass regions $m_{\chi_a} \geq 50$ GeV and $m_{H_a} \geq 100$ GeV.

In addition to the requirements in the preceding paragraph and the vacuum stability conditions in eq. (2.9), when selecting the inert scalars' parameters we take

into account also the Higgs mass which will be estimated at the one-loop level in section 5.5 and then limited to $m_h = (125.1 \pm 0.1)$ GeV, well within the ranges of the newest measurements [16, 17]. More specifically, we will therefore make the parameter choices

$$\begin{aligned} &0 < \lambda_{2a}, |\lambda_{3a}|, |\lambda_{4a}|, |\lambda_6|, |\lambda_7| < 3, \qquad \left|\mu_{2a}^2\right| < (800 \text{ GeV})^2, \\ &|\lambda_5| < 0.01 \,\text{Min}\left(\lambda_{2a}, |\lambda_{3a}|, |\lambda_{4a}|, |\lambda_6|, |\lambda_7|\right). \end{aligned} \tag{3.4}$$

The recently discovered Higgs boson may offer a window into physics beyond the SM. The presence of new particles can give rise to modifications to the standard decay modes of the Higgs and/or cause it to undergo exotic decays [18]. As data from the LHC will continue to accumulate with improving precision, they may uncover clues of new physics in the Higgs couplings or, otherwise, yield growing constraints on various models. Here we address some of the potential implications for our scenario of interest. Especially, the existing experimental information on the possible Higgs decay into invisible/nonstandard final states [19–23] and on the observed $h \to \gamma\gamma$ mode [17, 24] can supply further restrictions on the inert scalars.

The Higgs boson couples to a pair of them according to

$$\begin{aligned} \mathcal{L} \supset \frac{2h}{v} \big[&\left(\mu_{21}^2 - m_{H_1}^2\right) H_1^+ H_1^- + \left(\mu_{22}^2 - m_{H_2}^2\right) H_2^+ H_2^- \\ &+ \left(c_\theta^2 \mu_{21}^2 + s_\theta^2 \mu_{22}^2 - m_{\chi_1}^2\right) \chi_1^* \chi_1 + \left(c_\theta^2 \mu_{22}^2 + s_\theta^2 \mu_{21}^2 - m_{\chi_2}^2\right) \chi_2^* \chi_2 \\ &+ c_\theta s_\theta \left(\mu_{21}^2 - \mu_{22}^2\right) \left(\chi_1^* \chi_2 + \chi_2^* \chi_1\right) \big], \end{aligned} \tag{3.5}$$

from the $\mathcal{V}$ part of eq. (2.1). In view of the mass choices made above, it follows that the decay modes $h \to \chi_a^* \chi_b$, if kinematically allowed, contribute at tree level to the total width of the Higgs boson and are the leading channels into nonstandard final states in the model. Their rates have the form

$$\Gamma\left(h \to \chi_a^* \chi_b\right) = \frac{\left|C_{\chi_a^* \chi_b}\right|^2}{4\pi m_h^3 v^2} \sqrt{\left(m_h^2 - m_{\chi_a}^2 - m_{\chi_b}^2\right)^2 - 4 m_{\chi_a}^2 m_{\chi_b}^2}, \tag{3.6}$$

where

$$\begin{aligned} &C_{\chi_1^* \chi_1} = c_\theta^2 \mu_{21}^2 + s_\theta^2 \mu_{22}^2 - m_{\chi_1}^2, \qquad C_{\chi_2^* \chi_2} = c_\theta^2 \mu_{22}^2 + s_\theta^2 \mu_{21}^2 - m_{\chi_2}^2, \\ &C_{\chi_1^* \chi_2} = C_{\chi_2^* \chi_1} = c_\theta s_\theta \left(\mu_{21}^2 - \mu_{22}^2\right). \end{aligned} \tag{3.7}$$

The combined branching ratio of these decays is

$$\mathcal{B}\left(h \to \chi^* \chi'\right) = \frac{\sum_{a,b} \Gamma\left(h \to \chi_a^* \chi_b\right)}{\Gamma_h^{\text{SM}} + \sum_{a,b} \Gamma\left(h \to \chi_a^* \chi_b\right)}, \tag{3.8}$$

where Γ_h^{SM} is the SM Higgs total width and only channels satisfying $m_{\chi_a} + m_{\chi_b} < m_h$ contribute to the sums. Numerically, we adopt $\Gamma_h^{\text{SM}} = 4.08$ MeV [25] corresponding

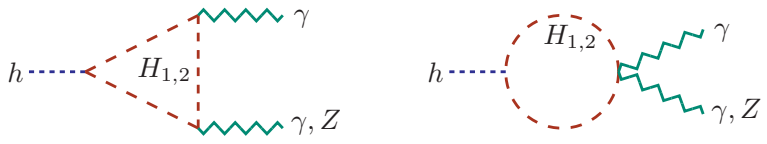

Figure 1. Feynman diagrams for the contributions of the new charged scalars $H^{\pm}_{1,2}$ to the Higgs boson decays $h \to \gamma\gamma$, and $h \to \gamma Z$. The triangle diagram with the gauge boson legs interchanged is not shown.

to $m_h = 125.1$ GeV. If these channels are open, we will require $\mathcal{B}\big(h \to \chi_a^* \chi_b\big) < 0.19$, based on the latest analysis of Higgs data [19–23].

The potential impact of the inert scalars can also be realized through loop diagrams. Of much interest are their contributions to the standard decay channels $h \to \gamma\gamma$ and $h \to \gamma Z$, which are already under investigation at the LHC. In the SM, they arise mainly from top-quark- and W-boson-loop diagrams. These modes receive additional contributions arising from the $H^{\pm}_{1,2}$-loop diagrams drawn in figure 1, with vertices from eqs. (3.1) and (3.5).[2] Their decay rates are readily obtainable from those in the case of only one inert doublet [26]. Thus we get

$$\Gamma(h \to \gamma\gamma) = \frac{\alpha^2 G_F m_h^3}{128\sqrt{2}\pi^3} \left| \frac{4}{3} A_{1/2}^{\gamma\gamma}(\kappa_t) + A_1^{\gamma\gamma}(\kappa_W) + \sum_{a=1}^{2} \frac{m_{H_a}^2 - \mu_{2a}^2}{m_{H_a}^2} A_0^{\gamma\gamma}\left(\kappa_{H_a}\right) \right|^2 , \tag{3.9}$$

$$\Gamma(h \to \gamma Z) = \frac{\alpha G_F^2 m_W^2 \left(m_h^2 - m_Z^2\right)^3}{64\pi^4 m_h^3} \left| \frac{6 - 16 s_{\rm w}^2}{3 c_{\rm w}} A_{1/2}^{\gamma Z}(\kappa_t, \lambda_t) + c_{\rm w} A_1^{\gamma Z}(\kappa_W, \zeta_W) \right.$$
$$\left. - \frac{1 - 2 s_{\rm w}^2}{c_{\rm w}} \sum_{a=1}^{2} \frac{m_{H_a}^2 - \mu_{2a}^2}{m_{H_a}^2} A_0^{\gamma Z}\left(\kappa_{H_a}, \zeta_{H_a}\right) \right|^2 , \tag{3.10}$$

where $\alpha = g^2 s_{\rm w}^2/(4\pi)$ is the fine-structure constant, the expressions for the form factors $A_{0,1/2,1}^{\gamma\gamma,\gamma Z}$ are available from ref. [27], the $A_0^{\gamma\gamma,\gamma Z}$ terms originate exclusively from the $H^{\pm}_{1,2}$ diagrams, $\kappa_X = 4m_X^2/m_h^2$, and $\zeta_X = 4m_X^2/m_Z^2$.

We can already test the new contributions to $h \to \gamma\gamma$, which has been observed at the LHC, unlike the γZ channel. For the $\gamma\gamma$ signal strengths, the ATLAS and CMS Collaborations measured $\sigma/\sigma_{\rm SM} = 1.17 \pm 0.27$ [24] and 1.13 ± 0.24 [17], respectively. These numbers need to be respected by the ratio of $\Gamma(h \to \gamma\gamma)$ to its SM value,

$$\mathcal{R}_{\gamma\gamma} = \frac{\Gamma(h \to \gamma\gamma)}{\Gamma(h \to \gamma\gamma)_{\rm SM}} \,. \tag{3.11}$$

[2] At the one-loop level, the charged (charged and neutral) inert scalars also induce $h \to \gamma C$ ($h \to ZC, CC$) involving the massless dark gauge boson C. These decay modes may be challenging to detect with C being invisible, as their rates are expected to be roughly of similar order to those of the $\gamma\gamma$ and γZ channels.

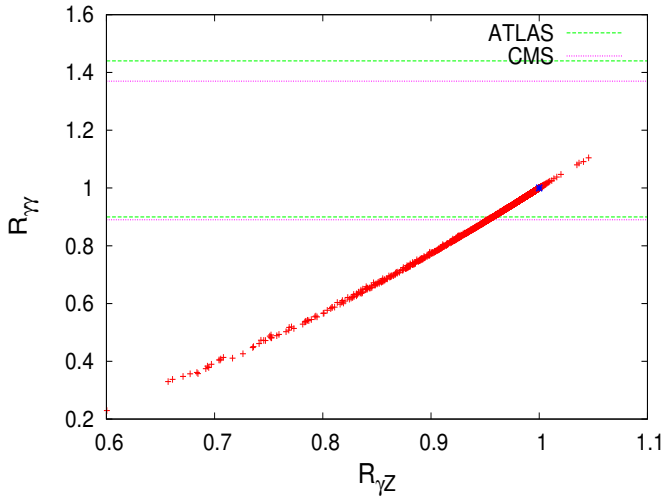

Figure 2. The effects of the new charged scalars $H^{\pm}_{1,2}$ on the ratios of the rates of Higgs decay channels $h \to \gamma\gamma$ and $h \to \gamma Z$ to their respective SM values for 5000 benchmark points as described in the text. The blue point marks the SM value. The region between the green (magenta) horizontal lines represents the one-sigma range of the ATLAS (CMS) data [17, 24].

Its γZ counterpart,

$$\mathcal{R}_{\gamma Z} = \frac{\Gamma(h \to \gamma Z)}{\Gamma(h \to \gamma Z)_{\rm SM}} \,, \tag{3.12}$$

will be probed by future experiments.

To illustrate the effects of the inert scalars on $\mathcal{R}_{\gamma\gamma}$ and $\mathcal{R}_{\gamma Z}$, and possible (anti)correlation between them, we display in figure 2 the distribution of 5000 benchmark points on the $(\mathcal{R}_{\gamma Z}, \mathcal{R}_{\gamma\gamma})$ plane which satisfy the vacuum stability requirements in eq. (2.9), the constraints from W and Z decays in eq. (3.3), and the parameter limitations in eq. (3.4). We notice that many of the $\mathcal{R}_{\gamma\gamma}$ values are close to 1 and within the allowed ranges from ATLAS and CMS. The plot also reveals that for the $\mathcal{R}_{\gamma\gamma}$ points compatible with the LHC data the values of $\Gamma(h \to \gamma Z)$ do not differ from its SM value by more than 10% or so. Furthermore, there is a positive correlation between $\mathcal{R}_{\gamma\gamma}$ and $\mathcal{R}_{\gamma Z}$, which is much like the situation in the case of only one inert doublet [26, 28, 29]. This can be checked experimentally when the γZ mode is observed in the future.

4 Electroweak Precision Tests

The interactions of the new doublets with the SM gauge bosons described by eq. (3.1) bring about modifications, ΔS and ΔT, to the so-called oblique electroweak parameters S and T which encode the effects of new physics not directly coupled to SM

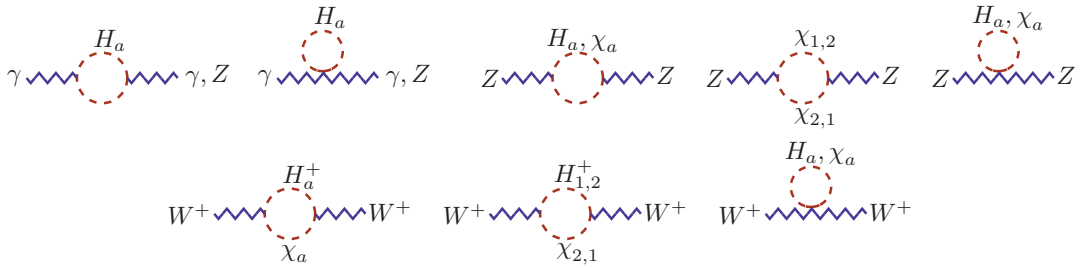

Figure 3. Feynman diagrams for the contributions of the inert scalar doublets to the oblique electroweak parameters ΔS and ΔT.

fermions [30]. At the one-loop level [3, 30]

$$\frac{\alpha\Delta S}{4c_{\rm w}^2 s_{\rm w}^2} = \frac{A_{ZZ}\left(m_Z^2\right) - A_{ZZ}(0)}{m_Z^2} - A'_{\gamma\gamma}(0) - \frac{c_{\rm w}^2 - s_{\rm w}^2}{c_{\rm w} s_{\rm w}} A'_{\gamma Z}(0),$$
$$\alpha\Delta T = \frac{A_{WW}(0)}{m_W^2} - \frac{A_{ZZ}(0)}{m_Z^2}, \tag{4.1}$$

where the functions $A_{XY}\left(q^2\right)$ can be extracted from the vacuum polarization tensors $\Pi_{XY}^{\mu\nu}\left(q^2\right) = A_{XY}\left(q^2\right) g^{\mu\nu} + \left[q^\mu q^\nu \text{ terms}\right]$ of the SM gauge bosons due to the new scalars' loop contributions, and $A'_{XY}(0) = \left[dA_{XY}\left(q^2\right)/dq^2\right]_{q^2=0}$. In our numerical analysis below, we will impose

$$\Delta S = 0.05 \pm 0.11, \qquad \Delta T = 0.09 \pm 0.13, \tag{4.2}$$

which are based on the results of a recent fit [31] to electroweak precision data for a Higgs mass $m_h = 125$ GeV.

The contributions of the inert scalars to ΔS and ΔT arise from the diagrams depicted in figure 3. After evaluating them, we arrive at[3]

$$\Delta S = \frac{1}{6\pi}\left[\ln\frac{m_{\chi_1} m_{\chi_2}}{m_{H_1} m_{H_2}} + s_{2\theta}^2 \frac{22 m_{\chi_1}^2 m_{\chi_2}^2 - 5 m_{\chi_1}^4 - 5 m_{\chi_2}^4}{6\left(m_{\chi_1}^2 - m_{\chi_2}^2\right)^2}\right.$$
$$\left. + s_{2\theta}^2 \frac{\left(m_{\chi_1}^2 + m_{\chi_2}^2\right)\left(m_{\chi_1}^4 - 4 m_{\chi_1}^2 m_{\chi_2}^2 + m_{\chi_2}^4\right)}{\left(m_{\chi_1}^2 - m_{\chi_2}^2\right)^3} \ln\frac{m_{\chi_1}}{m_{\chi_2}}\right], \tag{4.3}$$

$$\Delta T = \frac{1}{8\alpha\pi^2 v^2}\left[c_\theta^2 \mathcal{F}\left(m_{H_1}, m_{\chi_1}\right) + c_\theta^2 \mathcal{F}\left(m_{H_2}, m_{\chi_2}\right) + s_\theta^2 \mathcal{F}\left(m_{H_1}, m_{\chi_2}\right)\right.$$
$$\left. + s_\theta^2 \mathcal{F}\left(m_{H_2}, m_{\chi_1}\right) - 4 c_\theta^2 s_\theta^2 \mathcal{F}\left(m_{\chi_1}, m_{\chi_2}\right)\right], \tag{4.4}$$

where

$$\mathcal{F}(m,n) = \frac{m^2 + n^2}{2} - \frac{m^2 n^2}{m^2 - n^2}\ln\frac{m^2}{n^2}. \tag{4.5}$$

[3] Their counterparts in the case of only one inert scalar doublet were computed in Ref. [32].

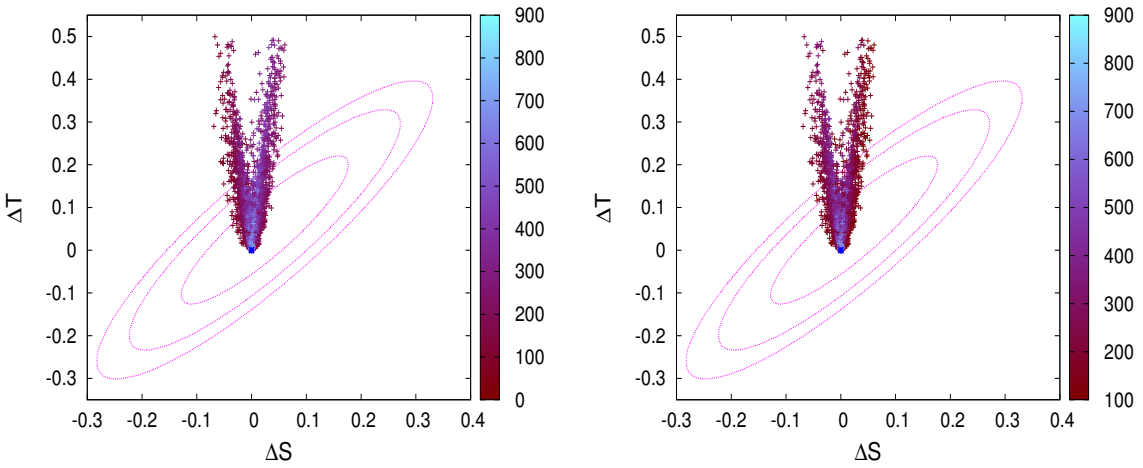

Figure 4. The contributions of the inert scalar doublets to the oblique electroweak parameters ΔS and ΔT for the 5000 benchmarks used previously. On the left panel, the palette belongs to the lighter neutral inert scalar's mass, m_{χ_1}, in GeV. On the right panel, the palette belongs to the lighter charged scalar mass, m_{H_1}, in GeV. The different contours represent 68%, 95%, and 99% confidence level, respectively. The blue point at (0,0) marks the SM value.

In figure 4, we present the distribution on the $(\Delta S, \Delta T)$ plane of the inert scalars' contributions for the 5000 benchmarks employed previously for figure 2. Evidently, it is possible for the masses of the charged scalars to be as small as 100 GeV and still be compatible with the electroweak precision measurements. However, we find that the lighter one of the inert neutral scalars, χ_1, must be heavier than about 90 GeV, which is a stronger condition than that inferred from the LEP constraint on the invisible width of the Z boson. This also makes the bound from the data on the Higgs invisible/nonstandard decay irrelevant.

5 Higgs Trilinear Coupling

Since the new scalars couple directly to the Higgs boson, their presence can cause its trilinear coupling, λ_{hhh}, to shift from its SM prediction. Such a modification could translate into detectable collider signatures, especially at a future e^+e^- machine such as the International Linear Collider [33] where the coupling can be measured with 20% precision or better at a center-of-mass energy $\sqrt{s} = 500$ GeV if the integrated luminosity is 500 fb^{-1}.

To derive the formula for the mass-dimension Higgs trilinear coupling in the presence of extra heavy particles, we follow the steps taken in ref. [34]. It is just the third derivative of the Higgs effective potential, namely

$$\lambda_{hhh} = \frac{\partial^3}{\partial \varphi^3} V_{\rm eff}^{T=0}(\varphi)\Big|_{\varphi=v}, \tag{5.1}$$

where φ is the classical Higgs field and $V_{\rm eff}^{T=0}(\varphi)$ is the potential evaluated at temperature $T=0$. We estimate the potential at the one-loop level in the so-called $\overline{\rm DR}'$ scheme [35, 36] where it has the form

$$V_{\rm eff}^{T=0}(\varphi) = \frac{\mu_1^2}{2}\varphi^2 + \frac{\lambda_1}{8}\varphi^4 + \sum_i n_i \frac{\left(m_i^2(\varphi)\right)^2}{64\pi^2}\left(\ln\frac{m_i^2(\varphi)}{\Lambda^2} - \frac{3}{2}\right). \tag{5.2}$$

In the sum above, the index i runs over all the contributing particles, n_i stands for the number of internal degrees of freedom of the ith particle, with a minus sign added if it is a fermion, $m_i^2(\varphi)$ is its field-dependent squared mass, and Λ is the renormalization scale which we choose to be the Higgs mass, $\Lambda = 125.1$ GeV. More explicitly, $n_h = 1$, $n_{\mathcal{G}} = n_Z = n_\gamma = 3$, $n_W = 6$, $n_t = -12$, and $n_{\chi_a} = n_{H_a} = 2$, where $\mathcal{G}$ refers to the Goldstone bosons. We have collected the formulas for the various relevant $m_i^2(\varphi)$ in appendix C.

At tree level we have $\mu_1^2 = -\lambda_1 v^2/2 \equiv \hat{\mu}_1^2$, but it receives the one-loop correction

$$\delta\mu_1^2 = -\frac{1}{32\pi^2 v}\sum_i n_i m_i^2 \dot{m}_i^2 \left(\ln\frac{m_i^2}{\Lambda^2} - 1\right)\Big|_{\varphi=v}, \tag{5.3}$$

which follows from $\partial V_{\rm eff}^{T=0}(\varphi)/\partial\varphi = 0$ set at $\varphi = v \simeq 246$ GeV, where $m_i^2 \equiv m_i^2(\varphi)$ and $\dot{m}_i^2 \equiv \partial m_i^2/\partial\varphi$. Then the Higgs mass at the one-loop level, which is nothing but the second derivative of $V_{\rm eff}^{T=0}(\varphi)$, is given by

$$m_h^2 = \lambda_1 v^2 + \sum_i \frac{n_i}{32\pi^2}\left[\left(\ddot{m}_i^2 m_i^2 - \frac{\dot{m}_i^2 m_i^2}{v} + \left(\dot{m}_i^2\right)^2\right)\ln\frac{m_i^2}{\Lambda^2} - \ddot{m}_i^2 m_i^2 + \frac{\dot{m}_i^2 m_i^2}{v}\right]\Bigg|_{\varphi=v}, \tag{5.4}$$

where the first term is the familiar tree-level contribution, the second term is the radiative one-loop correction, and $\ddot{m}_i^2 \equiv \partial^2 m_i^2/\partial\varphi^2$. Accordingly, with m_h^2 being fixed to its empirical value, as λ_1 is varied along with the other scalar couplings it can be bigger or smaller than its tree-level value $\hat{\lambda}_1 = m_h^2/v^2 \simeq 0.258$, depending on the size and sign of the loop contribution in eq (5.4).

Incorporating eq. (5.4) into eq. (5.1), one then obtains

$$\begin{aligned}\lambda_{hhh} = \frac{3m_h^2}{v} + \frac{1}{32\pi^2}\sum_{i=\rm all} n_i \Bigg\{\left[\dddot{m}_i^2 m_i^2 + 3\left(\dot{m}_i^2 - \frac{m_i^2}{v}\right)\left(\ddot{m}_i^2 - \frac{\dot{m}_i^2}{v}\right)\right]\ln\frac{m_i^2}{\Lambda^2} \\ + \frac{\left(\dot{m}_i^2\right)^3}{m_i^2} - \dddot{m}_i^2 m_i^2 + \frac{3m_i^2}{v}\left(\ddot{m}_i^2 - \frac{\dot{m}_i^2}{v}\right)\Bigg\}\Bigg|_{\varphi=v},\end{aligned} \tag{5.5}$$

where $\dddot{m}_i^2 \equiv \partial^3 m_i^2/\partial\varphi^3$. Its SM counterpart, $\lambda_{hhh}^{\rm SM}$, has the same formula, except that in the sum i runs over SM fields only.

According to eq. (5.5) and appendix C, the Higgs trilinear coupling is a function of the couplings $\lambda_{3a} + \lambda_{4a}$ and λ_{3a} of the inert neutral and charged scalars, respectively, to the SM Higgs doublet, i.e. through the field-dependent masses and their

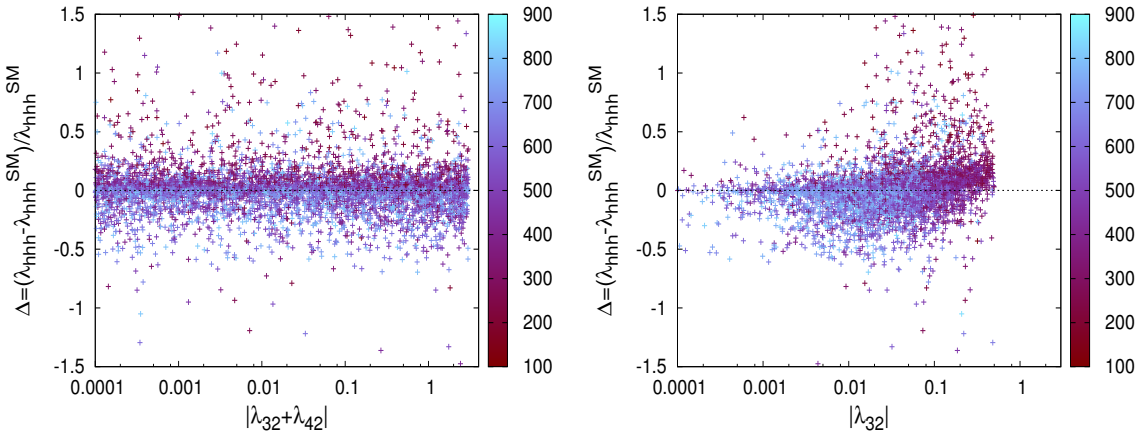

Figure 5. The changes of the Higgs trilinear coupling relative to its SM value versus the absolute values of the SM Higgs doublet couplings, $\lambda_{32}+\lambda_{42}$ and λ_{32}, to the heavy neutral (left) and the heavy charged (right) scalars, respectively. On the palettes, we read the heavy neutral (left) and charged (right) scalar masses in GeV.

derivatives. Since $\lambda_{3a,4a}$ are related to the scalars' physical masses via eqs. (2.4) and (2.6), the Higgs trilinear coupling also depends on them. To illustrate how the inert scalars' couplings and masses affect λ_{hhh}, we define the relative change

$$\Delta = \frac{\lambda_{hhh} - \lambda_{hhh}^{\rm SM}}{\lambda_{hhh}^{\rm SM}}, \tag{5.6}$$

with respect to the SM prediction. Then in figure 5 we graph Δ versus $|\lambda_{3a}+\lambda_{4a}|$ and $|\lambda_{3a}|$, respectively, for the 5000 benchmark points employed earlier. On the same plots we also show the mass distributions of the inert neutral and charged scalars, respectively.

It is clear that in the presence of the inert doublets the trilinear Higgs coupling can be enhanced or reduced by up to roughly 150% relative to the SM contribution to it. One realizes that, for either large or small (charged and/or neutral) scalar masses and couplings to the SM Higgs doublet, this enhancement or reduction of the trilinear coupling is the effect of the superposition of different contributions which could be constructive or destructive.

The new scalars impact can be further seen in figure 6, which illustrates their loop effects. Specifically, it displays the relative changes of the trilinear Higgs coupling, the Higgs mass, and the parameter μ_1^2 due to radiative corrections versus the Higgs quartic coupling λ_1, where

$$\delta\lambda_{hhh} = \lambda_{hhh} - 3\lambda_1 v, \qquad \delta m_h^2 = m_h^2 - \lambda_1 v^2, \tag{5.7}$$

$\delta\mu_1^2$ is defined in eq. (5.3), and $\mu_1^2 = \hat{\mu}_1^2 + \delta\mu_1^2$.

We remark that the Higgs quartic coupling, which at tree level is defined by the Higgs mass, can have a wide range from about 10^{-4} to 0.5. This is due to

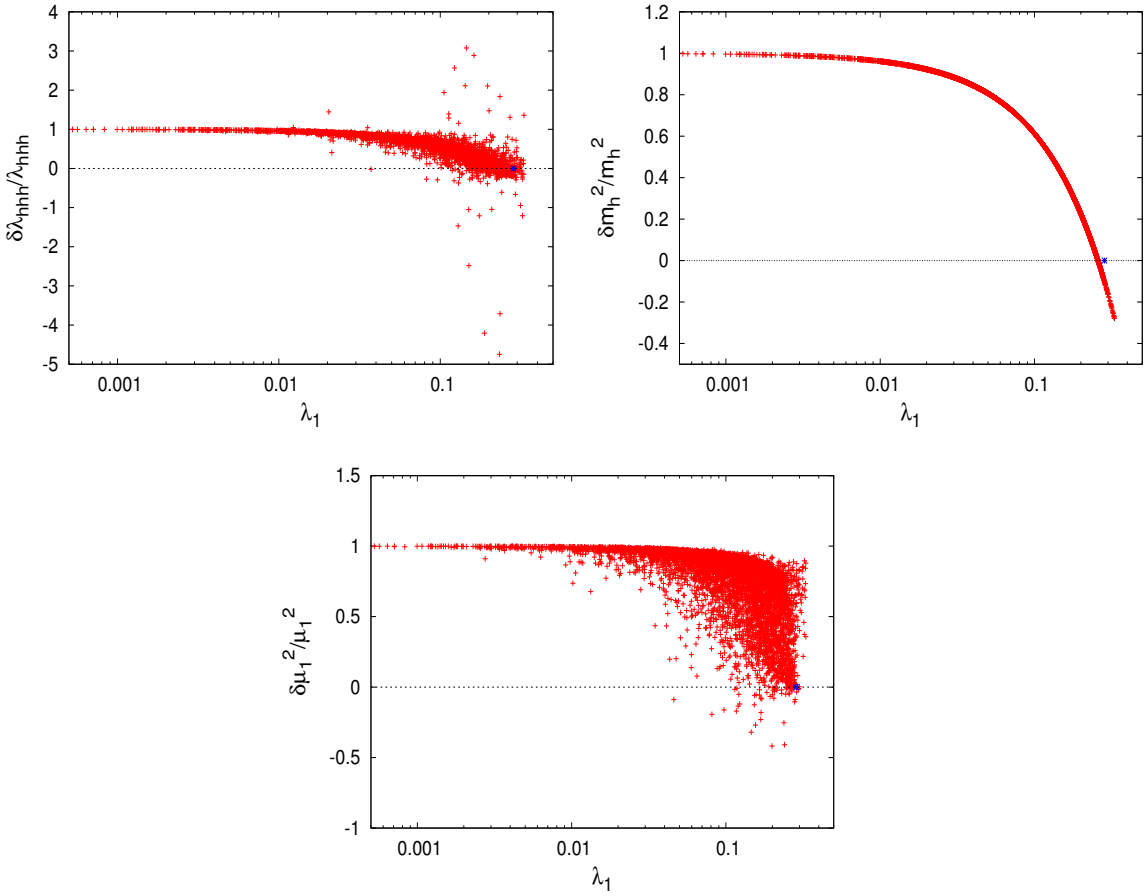

Figure 6. The relative changes of the trilinear Higgs coupling (left), the Higgs mass (right) and the μ_1^2 parameter (bottom) due to loop corrections versus the Higgs quartic coupling λ_1. The Higgs mass m_h is fixed to 125.1 GeV. The blue points represent the SM values.

the fact that much of the Higgs mass arises radiatively, as the right plot in figure 6 indicates. More precisely, m_h can be fully radiative for small λ_1 values or get a negative radiative correction for large λ_1 values, those greater than its tree-level one, $\hat{\lambda}_1$. One can see from the top-left and bottom plots in the figure that similar remarks could be made concerning λ_{hhh} and μ_1^2. In particular, each of these parameters may be fully radiative for small λ_1 and also can receive radiative corrections which are negative.

6 Electroweak Phase Transition

It is well-known that one of the reasons why the SM fails to produce successful baryogenesis [37] is the fact that the EWPT is not strong and consequently cannot suppress processes that violate the conservation of baryon plus lepton numbers, B+L, in the broken phase [38]. The suppression of anomalous B+L-violating processes in

the broken phase happens if the criterion for strongly first-order EWPT [39, 40],

$$v_c/T_c > 1, \tag{6.1}$$

is fulfilled, where v_c is the Higgs VEV at the critical temperature T_c at which the effective potential exhibits two degenerate minima, one at zero and the other at v_c. Both T_c and v_c are determined using the full thermal effective potential [41, 42]

$$V_{\text{eff}}(\varphi, T) = V_{\text{eff}}^{T=0}(\varphi) + \frac{T^4}{2\pi^2}\sum_i n_i J_{\mathsf{B},\mathsf{F}}\big(m_i^2(\varphi)/T^2\big) \tag{6.2}$$

at a finite temperature T, where

$$J_{\mathsf{B},\mathsf{F}}(r) = \int_0^\infty dx\, x^2 \ln\Big[1 \mp \exp\Big(-\sqrt{x^2+r}\Big)\Big], \tag{6.3}$$

the upper (lower) sign referring to a boson (fermion). To $V_{\text{eff}}(\varphi, T)$ one should add the so-called daisy (or ring) contribution [43]

$$V_{\text{ring}}(\varphi, T) = -\frac{T}{12\pi}\sum_i n_i\big(\tilde{m}_i^3(\varphi, T) - m_i^3(\varphi)\big) \tag{6.4}$$

which represents the leading term of higher-order loop corrections that may play an important role during the EWPT dynamics. In $V_{\text{ring}}(\varphi, T)$ the sum is over the scalar and longitudinal gauge degrees of freedom, $\tilde{m}_i^2(\varphi, T) = m_i^2(\varphi) + \Pi_i(T)$ are their thermal masses, and $\Pi_i(T)$ are the thermal parts of the self energies, which are collected in appendix C. To estimate $V_{\text{ring}}(\varphi, T)$, one performs the resummation of an infinite class of infrared-divergent multiloops diagrams, known as ring diagrams, that describes the dominant contribution of long distances and gives a significant contribution when (almost) massless states appear in the system. In our case, we will include this by following another approach. Rather than adding $V_{\text{ring}}(\varphi, T)$ to $V_{\text{eff}}(\varphi, T)$, we will replace in eq. (6.2) the field-dependent masses of the scalar and longitudinal gauge degrees of freedom with their thermal masses $\tilde{m}_i^2(\varphi, T)$.

In the criterion for a strong first-order phase transition, eq. (6.1), the critical temperature T_c is the value at which the two minima of the effective potential are degenerate,

$$\frac{\partial}{\partial\varphi}V_{\text{eff}}(\varphi, T_c)\Big|_{\varphi=v_c} = 0, \qquad V_{\text{eff}}(\varphi = v_c, T_c) = V_{\text{eff}}(\varphi = 0, T_c). \tag{6.5}$$

In the SM, this leads to a Higgs mass below 42 GeV [44], since the ratio v_c/T_c is inversely proportional to the Higgs quartic coupling λ_1. The strength of the EWPT can be improved if new bosonic degrees of freedom are invoked [45–48], which is the case we are investigating. It is clear from eq. (5.4) that for large values of the couplings and/or masses of the extra scalars, the one-loop corrections to the Higgs

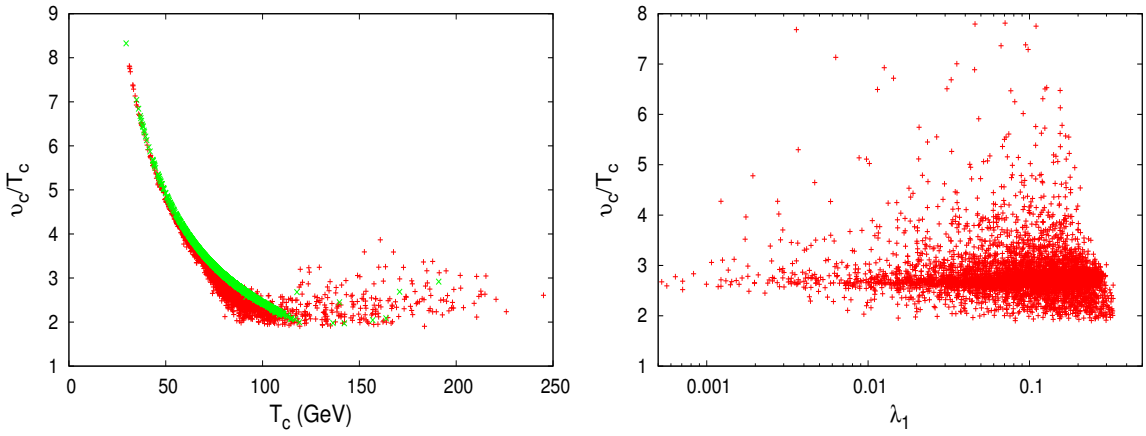

Figure 7. Left panel: v_c/T_c versus T_c, estimated with (red) and without (green) the daisy contribution. Right panel: v_c/T_c versus the Higgs quartic coupling λ_1, estimated by considering the daisy contribution.

mass could be significant, which allows the Higgs quartic coupling to be smaller and, therefore, fulfills the criterion in eq. (6.1) without conflicting with the recent Higgs mass measurements [16, 17]. Here, the relevant couplings are those of the Higgs doublet to the charged scalars, λ_{3a}, and to the neutral ones, $\lambda_{3a} + \lambda_{4a}$, in the limit $|\lambda_5| \ll |\lambda_{3a,4a}|$. The situation may be compared to those in similar setups [49–52] where extra scalars can help bring about a strongly first-order EWPT by (a) relaxing the Higgs quartic coupling λ_1 to as small as $\mathcal{O}(10^{-4})$ and (b) enhancing the value of the effective potential at the wrong vacuum at the critical temperature without suppressing the ratio v_c/T_c, which relaxes the severe bound on the mass of the SM Higgs.

The integral in eq. (6.3) is often approximated by a high temperature expansion. However, in order to take into account the effect of all the (heavy and light) degrees of freedom, we will evaluate them numerically.

With the same 5000 benchmark points used previously, in figure 7 we present v_c/T_c as a function of T_c and of the Higgs quartic coupling. It is obvious that strong first-order EWPT criterion is easily realized for the considered benchmarks, which all yield v_c/T_c larger than 2. Moreover, we find that the daisy contribution to the effective potential, that weakens the SM EWPT, does not play any role in the EWPT strength, but only barely delays the transition. One notices also that the EWPT strength is guaranteed here whatever the Higgs quartic coupling λ_1 is in the range shown, even for values larger than the tree-level one, $\hat{\lambda}_1$. This leads us to conclude that the EWPT is always strongly first-order due the reason (b) mentioned above, where the extra heavy scalars' existence makes the Higgs VEV slowly varying with respect to temperature and the wrong vacuum value, i.e. $V_{\text{eff}}(\varphi = 0, T)$, is evolving and increases with temperature.

We remark that due to the absence of a CP-violating phase in the potential $\mathcal{V}$ an additional source of CP violation has to be included in the Lagrangian of the more complete theory for it to be realistic for baryogensis. One possibility is to introduce dimension-six operators which couple the inert scalars to the top-quark mass and are suppressed by a new-physics scale that can be well above one TeV, in analogy to a scenario of electroweak baryogenesis from a singlet scalar [53].

7 Discussion & Conclusion

According to the analysis carried out in previous sections, the extra scalars can have important effects on the Higgs phenomenology and the electroweak phase transition if these particles are relatively light and the couplings to the SM Higgs doublet are large (λ_{3a} for charged scalars and $\lambda_{3a} + \lambda_{4a}$ for neutral ones). Therefore, from the 5000 benchmark points used previously, we extract those that simultaneously satisfy (i) the constraint from the measurements on the Higgs decay mode $h \to \gamma\gamma$, namely $0.9 < \mathcal{R}_{\gamma\gamma} < 1.37$, (ii) the electroweak precision tests, i.e. all the points inside the three ellipsoids in figure 4, and (iii) the criterion $v_c/T_c > 1$ for strongly first-order EWPT. As mentioned in section 4, the Higgs decay channel into a pair of inert scalars is closed for all the viable benchmarks and hence its experimental bound is not relevant. Here, we divide the points fulfilling the conditions (i,ii,iii) into three sets according to the ellipsoid to which they belong on the $(\Delta S, \Delta T)$ plane. The results are displayed in figure 8.

From the top panels in figure 8, one can see that the extra scalar masses do not exceed 900 GeV according to our parameter choices in eq. (3.4). The charged scalars could be light up to the LEP II bound (100 GeV), while the neutral scalars, which were supposed to be less constrained before, are now not allowed to be less than 120 GeV due to the electroweak precision tests in this model. From the bottom left panel, it is evident that the couplings of the Higgs doublet to the charged scalars, λ_{3a}, and to the neutral ones, $\lambda_{3a} + \lambda_{4a}$, could be both larger than 1 or smaller than 0.5. They could vary also within the whole considered range [0:3], or they could be almost equal in absolute values (i.e. close to the dashed curve). The bottom right plot in this figure reveal that, while strongly first-order EWPT occurs for all of the viable benchmark points, only for some of them is there a positive correlation between the EWPT strength and substantial enhancement of the Higgs trilinear coupling relative to the SM prediction as shown in ref. [10].

In conclusion, we have considered a scenario beyond the SM involving three scalar doublets and investigated a number of implications of the case where two of the doublets are inert and charged under a dark Abelian gauge symmetry. We looked at the effects of the new scalars on oblique electroweak parameters, the Higgs decay modes $h \to \gamma\gamma, \gamma Z$, and its trilinear coupling. We also examined how the inert scalars can induce strongly first-order EWPT. Taking into account various theoretical

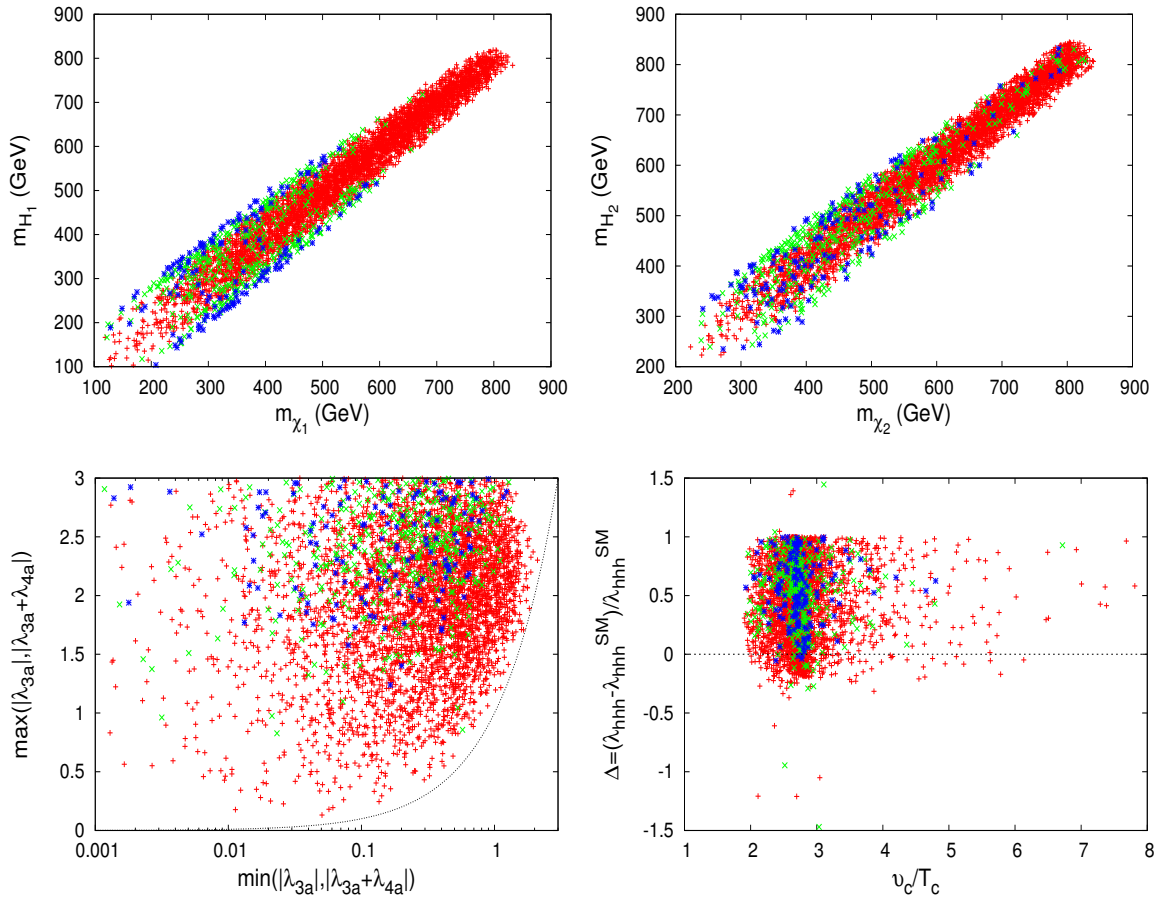

Figure 8. Top panels: the distribution of masses of the extra charged and neutral scalars under the assumptions described in the text. Bottom left panel: the strength distribution of the different quartic couplings of the Higgs doublet to the extra charged and neutral scalars; the dashed line represents the case where the couplings are equal in magnitude, i.e. $\text{Min}(|\lambda_{3a}|, |\lambda_{3a} + \lambda_{4a}|) = \text{Max}(|\lambda_{3a}|, |\lambda_{3a} + \lambda_{4a}|)$. Bottom right panel: the EWPT strength versus the relative enhancement of the Higgs trilinear coupling. The red, green, and blue points correspond to those inside the 99%, 95%, and 68% CL ellipsoids on the $(\Delta S, \Delta T)$ plane in figure 4.

and experimental constraints, we demonstrated that the viable parameter space can all accommodate strongly first-order EWPT and contains regions in which the Higgs trilinear coupling is enhanced/reduced by up to 150% compared to its SM value. Future experiments with sufficient precision can test the new scalars' effects that we have obtained on the Higgs decays $h \to \gamma\gamma, \gamma Z$ and trilinear coupling.

Acknowledgments

We would like to thank Masaya Kohda for helpful discussions. A.A. is supported by the Algerian Ministry of Higher Education and Scientific Research under the CNEPRU Project No. *D01720130042*. The work of G.F. and J.T. was supported in part by the research grant NTU-ERP-102R7701, the MOE Academic Excellence Program (Grant No. 102R891505), and the National Center for Theoretical Sciences of Taiwan.

A Vacuum stability conditions

We can rewrite the doublets Φ and $\eta_{1,2}$ and their products according to

$$\begin{aligned} &\Phi = f\hat{\Phi}, \qquad \hat{\Phi}^\dagger\hat{\Phi} = 1, \qquad \eta_a = e_a\hat{\eta}_a, \qquad \hat{\eta}_a^\dagger\hat{\eta}_a = 1\ , \qquad f, e_a > 0, \\ &\hat{\Phi}^\dagger\hat{\eta}_a\hat{\eta}_a^\dagger\hat{\Phi} = \rho_a, \qquad \hat{\eta}_1^\dagger\hat{\eta}_2\hat{\eta}_2^\dagger\hat{\eta}_1 = \rho', \qquad 0 \le \rho_a, \rho' \le 1. \end{aligned} \tag{A.1}$$

Assuming that λ_5 in eq. (2.2) is negligible compared to the other λ's, we can then express the part of $\mathcal{V}$ that is quartic in the doublets approximately as

$$\begin{aligned} \mathcal{V}_4 &= \tfrac{1}{2}\lambda_1 f^4 + \tfrac{1}{2}\lambda_{21}e_1^4 + \tfrac{1}{2}\lambda_{22}e_2^4 + \lambda_{31}f^2e_1^2 + \lambda_{32}f^2e_2^2 \\ &\quad + \ \lambda_{41}f^2e_1^2\rho_1 + \lambda_{42}f^2e_2^2\rho_2 + \lambda_6 e_1^2e_2^2 + \lambda_7 e_1^2e_2^2\rho' \\ &= \tfrac{1}{2}\begin{pmatrix} f^2 & e_1^2 & e_2^2 \end{pmatrix}\tilde{\lambda}\begin{pmatrix} f^2 \\ e_1^2 \\ e_2^2 \end{pmatrix}, \end{aligned} \tag{A.2}$$

where

$$\tilde{\lambda} = \begin{pmatrix} \lambda_1 & \lambda_{31} + \rho_1\lambda_{41} & \lambda_{32} + \rho_2\lambda_{42} \\ \lambda_{31} + \rho_1\lambda_{41} & \lambda_{21} & \lambda_6 + \rho'\lambda_7 \\ \lambda_{32} + \rho_2\lambda_{42} & \lambda_6 + \rho'\lambda_7 & \lambda_{22} \end{pmatrix}. \tag{A.3}$$

To ensure the stability of the vacuum, we need to derive relations among the λ's in $\mathcal{V}_4$, which dominates $\mathcal{V}$ at large fields, such that the minimum of $\mathcal{V}_4$ remains positive. This can be achieved using copositivity criteria [54], which in this case are applied to the minimum of $\tilde{\lambda}$. Since $\lambda_{4a,7}$ can be positive, zero, or negative and $0 \le \rho_a, \rho' \le 1$, we have

$$\tilde{\lambda}_{\min} = \begin{pmatrix} \lambda_1 & \lambda_{31} + \mathrm{Min}\,(0, \lambda_{41}) & \lambda_{32} + \mathrm{Min}\,(0, \lambda_{42}) \\ \lambda_{31} + \mathrm{Min}\,(0, \lambda_{41}) & \lambda_{21} & \lambda_6 + \mathrm{Min}\,(0, \lambda_7) \\ \lambda_{32} + \mathrm{Min}\,(0, \lambda_{42}) & \lambda_6 + \mathrm{Min}\,(0, \lambda_7) & \lambda_{22} \end{pmatrix}. \tag{A.4}$$

From the criteria for strictly copositive 3×3 matrices [55–57] then follow the conditions in eq. (2.9).

B Interaction terms for $\mathcal{S}_a$ and $\mathcal{P}_a$

The interaction terms of $\chi_{1,2}$ in eqs. (3.1) and (3.5) can be rewritten in terms of the real and imaginary components defined in eq. (2.7). Thus

$$\begin{aligned}
\mathcal{L} \supset\ & \frac{g}{2c_{\rm w}}\Big[c_{2\theta}\Big(\mathcal{P}_1\overset{\leftrightarrow}{\partial}^{\mu}\mathcal{S}_1 - \mathcal{P}_2\overset{\leftrightarrow}{\partial}^{\mu}\mathcal{S}_2\Big) + s_{2\theta}\Big(\mathcal{P}_1\overset{\leftrightarrow}{\partial}^{\mu}\mathcal{S}_2 + \mathcal{P}_2\overset{\leftrightarrow}{\partial}^{\mu}\mathcal{S}_1\Big)\Big]Z_{\mu} \\
& + \frac{ig}{2}\Big\{\Big[c_{\theta}H_1^{+}\overset{\leftrightarrow}{\partial}^{\mu}(\mathcal{S}_1 - i\mathcal{P}_1) + c_{\theta}H_2^{+}\overset{\leftrightarrow}{\partial}^{\mu}(\mathcal{S}_2 + i\mathcal{P}_2) \\
& \qquad + s_{\theta}H_1^{+}\overset{\leftrightarrow}{\partial}^{\mu}(\mathcal{S}_2 - i\mathcal{P}_2) - s_{\theta}H_2^{+}\overset{\leftrightarrow}{\partial}^{\mu}(\mathcal{S}_1 + i\mathcal{P}_1)\Big]W_{\mu}^{-} - \text{H.c.}\Big\} \\
& + \frac{g^2}{4}\big(\mathcal{S}_1^2 + \mathcal{P}_1^2 + \mathcal{S}_2^2 + \mathcal{P}_2^2\big)\left(\frac{Z^2}{2c_{\rm w}^2} + W^{+\mu}W_{\mu}^{-}\right) \\
& + \frac{h}{v}\big[\big(c_{\theta}^2\mu_{21}^2 + s_{\theta}^2\mu_{22}^2 - m_{\chi_1}^2\big)\big(\mathcal{S}_1^2 + \mathcal{P}_1^2\big) + \big(c_{\theta}^2\mu_{22}^2 + s_{\theta}^2\mu_{21}^2 - m_{\chi_2}^2\big)\big(\mathcal{S}_2^2 + \mathcal{P}_2^2\big) \\
& \qquad + s_{2\theta}\big(\mu_{21}^2 - \mu_{22}^2\big)\big(\mathcal{S}_1\mathcal{S}_2 + \mathcal{P}_1\mathcal{P}_2\big)\big]\,.
\end{aligned} \tag{B.1}$$

C Field-Dependent and Thermal Masses

To estimate the Higgs effective potential, one needs the field-dependent squared masses $m_i^2(\varphi)$ of all the contributing particles. One also requires the first, second, and third derivatives of $m_i^2(\varphi)$ to determine the counterterm $\delta\mu_1^2$ in eq. (5.3), the one-loop correction to the Higgs mass, and the enhancement of the Higgs trilinear coupling.

The field-dependent masses of the electroweak bosons and top quark have their SM values. For the other particles, $m_i^2(\varphi)$ are given by

$$\begin{aligned}
m_{\mathcal{G}}^2(\varphi) &= \mu_1^2 + \tfrac{1}{2}\lambda_1\varphi^2, & m_h^2(\varphi) &= \mu_1^2 + \tfrac{3}{2}\lambda_1\varphi^2, \\
m_{H_a}^2(\varphi) &= \mu_{2a}^2 + \tfrac{1}{2}\lambda_{3a}\varphi^2, & m_{\chi_{1,2}}^2(\varphi) &= \tfrac{1}{2}\Big(C_1 + C_2 \mp \sqrt{R}\Big), \\
C_a &= \mu_{2a}^2 + \tfrac{1}{2}(\lambda_{3a} + \lambda_{4a})\varphi^2, & R &= (C_1 - C_2)^2 + 4c^2, \quad c = \tfrac{1}{4}\,|\lambda_5|\,\varphi^2.
\end{aligned} \tag{C.1}$$

Hence the Goldstone bosons ($\mathcal{G}$) and the Higgs boson have the same field-dependent masses as their respective counterparts in the SM. The CP-even and CP-odd neutral scalars mix, leading to equal-mass eigenstates according to eq. (2.8).

It is simple to get the first, second, and third derivatives of $m_i^2(\varphi)$ from eq. (C.1).

For completeness, here we supply them explicitly:

$$\begin{aligned}
\dot{m}^2_{\mathcal{G}}(\varphi) &= \lambda_1\varphi, \quad \dot{m}^2_h(\varphi) = 3\lambda_1\varphi, \quad \dot{m}^2_{H_a}(\varphi) = \lambda_{3a}\varphi, \\
\dot{m}^2_{\chi_{1,2}}(\varphi) &= \frac{1}{2}\left(\dot{C}_1 + \dot{C}_2 \mp \frac{\dot{R}}{2\sqrt{R}}\right), \\
\dot{C}_a &= (\lambda_{3a} + \lambda_{4a})\,\varphi, \quad \dot{c} = \tfrac{1}{2}\,|\lambda_5|\,\varphi, \\
\dot{R} &= 2\left(\dot{C}_1 - \dot{C}_2\right)(C_1 - C_2) + 8\dot{c}c,
\end{aligned} \tag{C.2}$$

$$\begin{aligned}
\ddot{m}^2_{\mathcal{G}}(\varphi) &= \lambda_1, \quad \ddot{m}^2_h(\varphi) = 3\lambda_1, \quad \ddot{m}^2_{H_a}(\varphi) = \lambda_{3a}, \\
\ddot{m}^2_{\chi_{1,2}}(\varphi) &= \frac{1}{2}\left(\ddot{C}_1 + \ddot{C}_2 \mp \frac{\ddot{R}}{2\sqrt{R}} \pm \frac{\dot{R}^2}{4\sqrt{R^3}}\right), \\
\ddot{C}_a &= \lambda_{3a} + \lambda_{4a}, \quad \ddot{c} = \tfrac{1}{2}\,|\lambda_5|\,, \\
\ddot{R} &= 2\left(\dot{C}_1 - \dot{C}_2\right)^2 + 2\left(\ddot{C}_1 - \ddot{C}_2\right)(C_1 - C_2) + 8\dot{c}^2 + 8\ddot{c}c,
\end{aligned} \tag{C.3}$$

$$\begin{aligned}
\dddot{m}^2_{\mathcal{G}}(\varphi) &= \dddot{m}^2_h(\varphi) = \dddot{m}^2_{H_a}(\varphi) = \dddot{C}_a = \dddot{c} = 0, \\
\dddot{m}^2_{\chi_{1,2}}(\varphi) &= \mp\frac{1}{4\sqrt{R}}\left(\dddot{R} - \frac{3\dot{R}\ddot{R}}{2R} + \frac{3\dot{R}^3}{4R^2}\right), \\
\dddot{R} &= 6\left(\ddot{C}_1 - \ddot{C}_2\right)\left(\dot{C}_1 - \dot{C}_2\right) + 24\ddot{c}\dot{c}.
\end{aligned} \tag{C.4}$$

The thermal mass $\tilde{m}_i(\varphi, T)$ is related to $m_i^2(\varphi)$ by $\tilde{m}_i^2(\varphi, T) = m_i^2(\varphi) + \Pi_i(T)$, where $\Pi_i(T)$ is the thermal part of the self energy. For the scalar and electroweak bosons [58]

$$\begin{aligned}
\Pi_\Phi &= \left(6\lambda_1 + \frac{9}{2}g^2 + \frac{3}{2}g_Y^2 + 3y_t^2 + 4\lambda_{31} + 2\lambda_{41} + 4\lambda_{32} + 2\lambda_{42}\right)\frac{T^2}{12}, \\
\Pi_{\eta_a} &= \left(\frac{9}{2}g^2 + \frac{3}{2}g_Y^2 + 4\lambda_{3a} + 2\lambda_{4a} + 6\lambda_{2a} + 4\lambda_6 + 2\lambda_7 + \frac{3}{2}\mathcal{Q}^2_{\eta_a}g_D^2\right)\frac{T^2}{12}, \\
\Pi_W &= \frac{17}{6}g^2T^2, \quad \Pi_B = \frac{11}{16}g_Y^2T^2,
\end{aligned} \tag{C.5}$$

where y_t denotes the top-quark Yukawa coupling and $\mathcal{Q}_{\eta_a} = \mathcal{Q}_C\eta_a$ is the charge of the inert doublet η_a under $\mathrm{U}(1)_D$.

References

[1] G. Aad *et al.* [ATLAS Collaboration], Phys. Lett. B **716**, 1 (2012) [arXiv:1207.7214 [hep-ex]].

[2] S. Chatrchyan *et al.* [CMS Collaboration], Phys. Lett. B **716**, 30 (2012) [arXiv:1207.7235 [hep-ex]].

[3] K.A. Olive *et al.* [Particle Data Group Collaboration], Chin. Phys. C **38**, 090001 (2014).

[4] J.F. Gunion, H.E. Haber, G.L. Kane, and S. Dawson, *The Higgs Hunter's Guide* (Westview Press, Colorado, 2000).

[5] G.C. Branco, P.M. Ferreira, L. Lavoura, M.N. Rebelo, M. Sher, and J.P. Silva, Phys. Rept. **516**, 1 (2012) [arXiv:1106.0034 [hep-ph]].

[6] I.P. Ivanov, V. Keus, and E. Vdovin, J. Phys. A **45**, 215201 (2012) [arXiv:1112.1660 [math-ph]].

[7] V. Keus, S.F. King, and S. Moretti, JHEP **1401**, 052 (2014) [arXiv:1310.8253 [hep-ph]].

[8] V. Keus, S.F. King, S. Moretti, and D. Sokolowska, JHEP **1411**, 016 (2014) [arXiv:1407.7859 [hep-ph]].

[9] E. Ma, I. Picek, and B. Radovcić, Phys. Lett. B **726**, 744 (2013) [arXiv:1308.5313 [hep-ph]].

[10] S. Kanemura, Y. Okada, and E. Senaha, Phys. Lett. B **606**, 361 (2005) [hep-ph/0411354].

[11] C.W. Chiang and T. Yamada, arXiv:1404.5182 [hep-ph].

[12] K. Fuyuto and E. Senaha, Phys. Rev. D **90**, no. 1, 015015 (2014) [arXiv:1406.0433 [hep-ph]].

[13] S. Kanemura, T. Kasai, and Y. Okada, Phys. Lett. B **471**, 182 (1999) [hep-ph/9903289].

[14] S.Y. Ho and J. Tandean, Phys. Rev. D **89**, 114025 (2014) [arXiv:1312.0931 [hep-ph]].

[15] E. Ma, Phys. Rev. D **73**, 077301 (2006) [hep-ph/0601225].

[16] G. Aad *et al.* [ATLAS Collaboration], Phys. Rev. D **90**, 052004 (2014) [arXiv:1406.3827 [hep-ex]].

[17] CMS Collaboration, Report No. CMS-PAS-HIG-14-009, July 2014.

[18] D. Curtin, R. Essig, S. Gori, P. Jaiswal, A. Katz, T. Liu, Z. Liu and D. McKeen *et al.*, Phys. Rev. D **90**, 075004 (2014) [arXiv:1312.4992 [hep-ph]].

[19] A. Falkowski, F. Riva, and A. Urbano, JHEP **1311**, 111 (2013) [arXiv:1303.1812 [hep-ph]].

[20] P.P. Giardino, K. Kannike, I. Masina, M. Raidal, and A. Strumia, JHEP **1405**, 046 (2014) [arXiv:1303.3570 [hep-ph]].

[21] J. Ellis and T. You, JHEP **1306**, 103 (2013) [arXiv:1303.3879 [hep-ph]].

[22] G. Belanger, B. Dumont, U. Ellwanger, J.F. Gunion, and S. Kraml, Phys. Rev. D **88**, 075008 (2013) [arXiv:1306.2941 [hep-ph]].

[23] K. Cheung, J. S. Lee and P. Y. Tseng, Phys. Rev. D **90** (2014) 9, 095009 [arXiv:1407.8236 [hep-ph]].

[24] G. Aad *et al.* [ATLAS Collaboration], Phys. Rev. D **90** (2014) 11, 112015 [arXiv:1408.7084 [hep-ex]].

[25] https://twiki.cern.ch/twiki/bin/view/LHCPhysics/CERNYellowReportPageBR3.

[26] S.Y. Ho and J. Tandean, Phys. Rev. D **87**, 095015 (2013) [arXiv:1303.5700 [hep-ph]].

[27] C.S. Chen, C.Q. Geng, D. Huang, and L.H. Tsai, Phys. Rev. D **87**, 075019 (2013) [arXiv:1301.4694 [hep-ph]].

[28] B. Swiezewska and M. Krawczyk, Phys. Rev. D **88**, no. 3, 035019 (2013) [arXiv:1212.4100 [hep-ph]].

[29] A.D. Banik and D. Majumdar, Eur. Phys. J. C **74**, no. 11, 3142 (2014) [arXiv:1404.5840 [hep-ph]].

[30] M.E. Peskin and T. Takeuchi, Phys. Rev. D **46**, 381 (1992).

[31] M. Baak *et al.* [Gfitter Group Collaboration], Eur. Phys. J. C **74**, no. 9, 3046 (2014) [arXiv:1407.3792 [hep-ph]].

[32] R. Barbieri, L.J. Hall, and V.S. Rychkov, Phys. Rev. D **74**, 015007 (2006) [hep-ph/0603188].

[33] H. Baer, et al., '*Physics at the International Linear Collider*', available at: http://lcsim.org/papers/DBDPhysics.pdf

[34] A. Ahriche, A. Arhrib and S. Nasri, JHEP **1402** (2014) 042 [arXiv:1309.5615 [hep-ph]].

[35] A.B. Lahanas and D.V. Nanopoulos, Phys. Rept. **145**, 1 (1987).

[36] S.P. Martin, Phys. Rev. D **65**, 116003 (2002) [hep-ph/0111209].

[37] V.A. Kuzmin, V.A. Rubakov, and M.E. Shaposhnikov, Phys. Lett. B **155**, 36 (1985).

[38] M. Trodden, Rev. Mod. Phys. **71**, 1463 (1999) [hep-ph/9803479].

[39] M.E. Shaposhnikov, Nucl. Phys. B **287**, 757 (1987).

[40] M. E. Shaposhnikov, Nucl. Phys. B **299**, 797 (1988).

[41] L. Dolan and R. Jackiw, Phys. Rev. D **9**, 3320 (1974).

[42] S. Weinberg, Phys. Rev. D **9**, 3357 (1974).

[43] M.E. Carrington, Phys. Rev. D **45**, 2933 (1992).

[44] A.I. Bochkarev and M.E. Shaposhnikov, Mod. Phys. Lett. A **2**, 417 (1987).

[45] A. Ahriche and S. Nasri, Phys. Rev. D **83**, 045032 (2011) [arXiv:1008.3106 [hep-ph]].

[46] T.A. Chowdhury, M. Nemevsek, G. Senjanovic, and Y. Zhang, JCAP **1202**, 029 (2012) [arXiv:1110.5334 [hep-ph]].

[47] D. Borah and J.M. Cline, Phys. Rev. D **86**, 055001 (2012) [arXiv:1204.4722 [hep-ph]].

[48] G. Gil, P. Chankowski and M. Krawczyk, Phys. Lett. B **717**, 396 (2012) [arXiv:1207.0084 [hep-ph]].

[49] A. Ahriche and S. Nasri, JCAP **1307**, 035 (2013) [arXiv:1304.2055].

[50] A. Ahriche, Phys. Rev. D **75**, 083522 (2007) [hep-ph/0701192].

[51] A. Ahriche and S. Nasri, Phys. Rev. D **85**, 093007 (2012) [arXiv:1201.4614 [hep-ph]].

[52] A. Ahriche, K.L. McDonald and S. Nasri, in preparation.

[53] J.M. Cline and K. Kainulainen, JCAP **1301**, 012 (2013) [arXiv:1210.4196 [hep-ph]].

[54] K. Kannike, Eur. Phys. J. C **72**, 2093 (2012) [arXiv:1205.3781 [hep-ph]].

[55] K. Hadeler, Linear Algebra Appl. **49**, 79 (1983).

[56] G. Chang and T.W. Sederberg, Comput. Aided Geom. Des. **11**(1), 113 (1994).

[57] L. Ping and F.Y. Yu, Linear Algebra Appl. **194**, 109 (1993).

[58] J.I. Kapusta and C. Gale, *Finite-temperature field theory: Principles and applications* (Cambridge University Press, Cambridge, 2006).